Impact of large scale photovoltaic generation on voltage stability in distribution networks

Abdelaziz Salah Saidi[1,2], **Khadija Ben-Kilani**[1], **Mohamed Elleuch**[1]

1. Electric Systems Laboratory, National Engineering School of Tunis ENIT Tunis, Tunisia

khadijakilani@yahoo.fr

2. King Khalid University, Electrical Engineering Department, Abha, Saudi Arabia

asaidi@kku.edu.sa

ABSTRACT. *This paper investigates the impact of integrating large scale photovoltaic power on voltage stability in radial distribution networks. Detailed modeling of the photovoltaic systems is presented. The study is based on bifurcation diagrams of photovoltaic generation, load flow analysis, short circuits, photovoltaic farm disconnections and loading conditions. Maximum penetration levels of solar photovoltaic generation are examined using bifurcation diagrams. The study considers is a utility 53 buses radial distribution network. Several aspects are presented and discussed.*

RÉSUMÉ. *L'évolution des réseaux électriques est marquée par des variations continues de leur topologie. En particulier l'intégration des sources renouvelables de plus en plus importantes a soumis ces réseaux à de nouvelles contraintes d'exploitation. A titre d'exemple, les systèmes photovoltaïques (PV) posent de nouveaux problèmes de stabilité aussi bien statique que dynamique, qui ne cessent d'évoluer avec l'accroissement des puissances installées. En effet, l'intégration de ces fermes photovoltaïques influe sur les caractéristiques électriques de fonctionnement du réseau en régime statique, et présente aussi un impact sur son comportement dynamique. Cet article porte sur l'impact d'une intégration massive de l'énergie photovoltaïque sur la stabilité statique et dynamique du réseau de distribution tunisien. Pour cela nous avons mené une étude statique basée sur les diagrammes de bifurcation de tension. Ensuite nous avons entamé le régime transitoire dans un tel système en cas de base et en cas de pénétration photovoltaïque maximale.*

KEYWORDS: *photovoltaic generator, radial distribution network, voltage stability, photovoltaic penetration, bifurcation diagram, saddle-node bifurcation.*

MOTS-CLÉS : *stabilité de tension, système photovoltaique, diagramme de bifurcation, stabilité transitoire.*

DOI:10.3166/EJEE.18.117-138

1. Introduction

Solar Photo-Voltaic Generators (SPVGs) are attractive sources of renewable energy for electric power generation due to their relatively small size and noiseless operation. Their applications have significantly increased all over the world. By 2013, approximately 139 GW of SPVGs had been installed worldwide (Ren, 2014).

Many previous works have examined the effects of increased penetration of renewable energy into power systems, especially the intermittent type, on power system stability. In the most part, the focus has been on wind energy (Erlich *et al.*, 2006) and (Gautam *et al.*, 2009). It has been argued that if proper controls are used, integration of wind energy would not significantly affect system stability (Gautam *et al.*, 2011) and (Muljadi *et al.*, 2008).

Nonetheless, the increased penetration levels of photovoltaic plants are raising concerns to utilities due to possible negative impacts on power system stability (Tan *et al.*, 2004), (Wang *et al.*, 2008) and (Xu *et al.*, 2009). When operated in parallel with conventional synchronous generators, SPVGs present new challenges to stability, operation and control of the power system and its components (Paladin, 2011). In particular, when SPVGs are integrated in distribution medium voltage distribution networks, nodal voltage stability ought to be affected. Voltage instability is outlined as the incapability of network to maintain satisfactory voltage levels throughout the network during different operating conditions. Voltage instability occurs when short or long term disturbances cause an unmanageable and progressive drop in voltage level (Lof *et al.*, 1993) and (Ajjarapu *et al.*, 1998). The key cause of voltage collapse is the incapability of network to supply the required reactive power. Thus, this issue needs to be methodically analyzed especially with the presence of large scale SPVGs.

Canova *et al.* (2009) examined the electrical impact of solar photovoltaic penetration at the distribution level, and concluded that these plants may affect the voltage profile if they are installed in rural radial lines. In (Kakimoto *et al.*, 2011), a voltage control scheme is proposed to avoid voltage problems in distribution networks. The impact of small SPVGs units on the operation of distribution systems was analyzed in (Thomson *et al.*, 2007), where it is indicated that considerable penetration of micro-generation may be accommodated safely without major modification to the system control. A correlation index is introduced in (Marinopoulos *et al.*, 2011) to evaluate the impact of solar photovoltaic units on real power losses in distribution systems. Tamimi *et al.* (2013) presented a comparative investigation of SPVGs effect on system stability at different penetration levels. The impact is examined through eigenvalue, voltage stability and transient stability analyses using real network data pertaining to Ontario and its neighboring systems. Tan (2007) described the impact on the power system of a large-scale penetration of photovoltaic generation. The dynamic response of a photovoltaic generation system to rapid change in irradiance was analyzed. Different types of voltage control techniques used to mitigate the negative effects of rapid changes in irradiance are

investigated using simulation. The static voltage stability of the power system with large-scale photovoltaic penetration is presented in (Rakibuzzaman *et al.*, 2012). The results in this study indicate that the SPVGs location, size and the way they are integrated, i.e., concentrated or dispersed, have profound impact on system static voltage stability. The paper of (Khan *et al.*, 2013) has shown the impact of photovoltaic generation on Bangladesh power system stability. Simulation results of static voltage stability in Bangladesh power system show SPVGs of different sizes at different zones has improved the voltage collapse point near the bus and loading margin. The paper of (Liu *et al.*, 2010) investigates the impact of SPVGs on power system small signal stability using modal analysis and time-domain simulation. The study results show that the presence of SPVGs can change the mode shape of the inter-area mode for the synchronous generators that are not displaced by SPVGs. The simulation results also show that increased SPVGs can have beneficial effect on small signal stability depending on the location and penetration level of solar photovoltaic generation and the dispatch of the existing synchronous generators.

This paper is also a part of the previously mentioned research and our objective is to examine the impact of penetration of solar photovoltaic generation on the steady state and dynamic behaviour of the radial Tunisian distribution network voltage stability.

The next section explores modeling of solar photovoltaic units, followed by a formulation of the various studies and methodology. The radial Tunisian distribution network is also briefly described in Section 3.1. Results and discussions are presented in Section 3.2 to 3.5. Finally, section 4 highlights the main conclusions of the paper.

2. Dynamic models of a solar photovoltaic unit

The solar photovoltaic cells generate a DC current which is converted into AC current by power electronics inverter control. The typical structure of a grid connected SPVG unit is shown in Figure 1. Its main subsystems are the photovoltaic array, the DC/DC and DC/AC converters, and the associated controls (converter and overall system) (CIGRE, 2000). The remaining system components, i.e. dc bus, inverter and grid-connection devices, are similar to those found in some other distributed generators such as variable speed wind turbines, and therefore the dynamic modeling requirements are similar (CIGRE, 2000).

According to the North American Electric Reliability Corporation (NERC, 2010), the SPVG model can be based on the grid-side model of certain types of wind turbine generators (WTG) that have a similar interfacing structure (Type 4 WTG), since SPVGs are typically connected to the grid through a converter. Figure 2 shows a Type 4 WTG WECC generic model where all the power generated is processed through the power converter, which serves as a buffer between the generator and the

grid, and controls the reactive power output and/or the voltage at the point of common coupling (PCC).

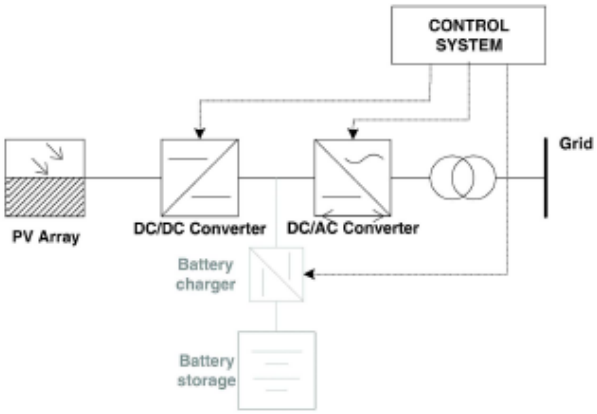

Figure 1. Typical structure of a grid connected SPVG (CIGRE, 2000)

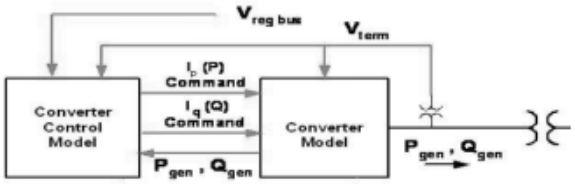

Figure 2. Type 4 WTG general block diagram (WECC, 2010)

The distributed SPVG units are modeled as constant PV or PQ generators depending on the chosen control mode and their capabilities depicted in Figures 3 and 4 for Models 1 and 2, respectively (Erlich *et al.*, 2006).

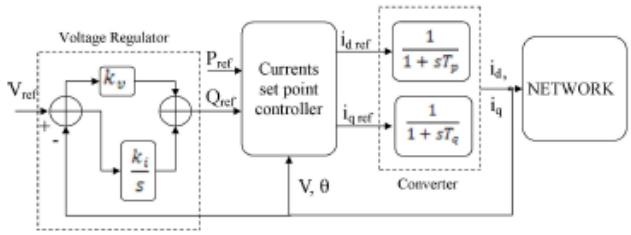

Figure 3. SPVG Model 1 block diagram including the converter

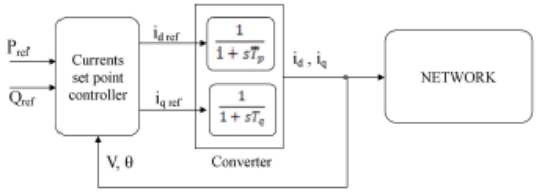

Figure 4. SPVG Model 2 block diagram including the converter

The IEEE guidelines for interconnection of distributed resources suggest connecting SPVGs at unity power factor (IEEE, 2000). Currently most inverters used in PV power conversion are designed to operate at unity power factor (Yun *et al.*, 2007) and (Yun *et al.*, 2004). In this paper too, the solar photovoltaic generators are assumed to be constant active power sources operating at unity power factor (i.e. the maximum and minimum reactive power limits of the generator are set to zero) and the model used is model 2.

The SPVG possessing dynamic components as characterized below:

$$\frac{di_d}{dt} = \frac{\left(Q_{ref}.\cos(t) - P_{ref}.sin(t)\right)/V - i_d}{T_p} \tag{1}$$

$$\frac{di_q}{dt} = \frac{\left(P_{ref}.\cos(t) + Q_{ref}.sin(t)\right)/V - i_q}{T_q} \tag{2}$$

In these models, the current set points can be obtained based on the desired active and reactive powers and measured terminal of voltages in the dq reference frame as follows:

$$\begin{bmatrix} i_d \\ i_q \end{bmatrix} = \begin{bmatrix} V_d & V_q \\ V_q & -V_d \end{bmatrix}^{-1} \begin{bmatrix} P \\ Q \end{bmatrix} \tag{3}$$

Where the notations carry their standard meanings as in (Tamimi *et al.,* 2013). In Figure 4, the reference value for reactive power is obtained based on the set-point and actual voltage values through a PI controller (Ko *et al.,* 2007).

At each bus *i*, the injected complex power $P_i + jQ_i$ must balance the algebraic sum of the specified power supply $P_{Gi}^{sp} + jQ_{Gi}^{sp}$, and power demand $P_{Li}^{sp} + jQ_{Li}^{sp}$. The active and reactive network equations are given by (4) and (5) respectively:

$$P_{Gi}^{sp} - P_{Li}^{sp} = \sum_{j=1}^{N} Y_{ij} V_i V_j cos\left(\alpha_i - \alpha_j - \theta_{ij}\right) \tag{4}$$

$$Q_{Gi}^{sp} - Q_{Li}^{sp} = \sum_{j=1}^{N} Y_{ij} V_i V_j sin(\alpha_i - \alpha_j - \theta_{ij}) \quad (5)$$

Where $\overline{V_i} = V_i \angle \alpha_i$ is the voltage at the i^{th} bus, $\overline{Y_{ij}} = Y_{ij} \angle \theta_{ij}$ are the elements *(i,j)* of the network admittance matrix and N is the total number of network buses.

3. Numerical studies

All numerical studies were carried out using the PSAT (Milano, 2005), which is a MATLAB-based toolbox for power system studies. It includes power flow, continuation power flow, optimal power flow, small-signal stability analysis and time domain simulation tools. This toolbox also provides a complete graphical interface and a SIMULINK-based one-line network editor.

3.1. System description

The configuration of a distribution system which is under study is shown in Figure 5. It is characterized by short lengths of transmission lines do not exceed two kilometers. The system has 53 buses, 2 generators, 51 loads, 1 transformer and 51 branches with base values 100 MVA, and 33 kV. The total system loading in the base case is 12.10 MW and 3.95 MVAR, with the loads being represented using constant power loads. The distribution network operates at one voltage level 33 kV. The synchronous generator connected to bus 52, is equipped with a Turbine Governor and an Automatic Voltage Regulator, the main power station of bus 53 is chosen as the slack bus. The solar photovoltaic generators designated PV1, PV2, PV3 are connected to buses 13, 18 and 46 respectively, and the maximum installed photovoltaic power is 12 MW and operating at unit power factor. The solar irradiation is assumed constant throughout the analysis. The model parameters used in Figure 5 is as follows: Q_G = 0.0MVAr, and $T_d = T_q$ = 15ms.

The goal of these simulations is to evaluate the dynamic performance of the voltage and the transient stability of a power system integrating three photovoltaic farms. The study of voltage stability is based on the bifurcation diagrams with the bifurcation parameter is the power generated by the photovoltaic generators in base case and in case of holidays. The study of the stability of the network is completed by an analysis of transient stability. For this purpose, worst-case scenarios are considered in base and at maximum photovoltaic penetration case. We first test the system transient response to a sudden photovoltaic loss: disconnection of all photovoltaic farms and disconnection of the most loaded bus ‘26’. Then, faulted voltage profiles are applied at the connection bus of the photovoltaic generator. Lastly three phase short circuit faults are applied at a regular transmission network

bus (load bus '26'). Through these studies, it will be possible to determine whether credible disturbances could lead to voltage collapse over parts of the system or to steady state instabilities.

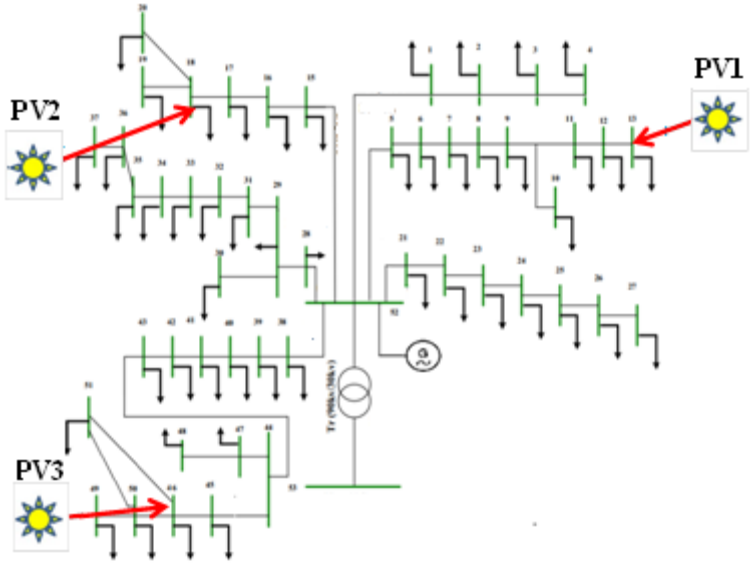

Figure 5. Single line diagram of a distribution system connected SPVG

3.2. Methodology

The proposed system model comprises a conventional power plant and photovoltaic generator as depicted in Figure 5. The transmission network is represented by a general π model. The overall system model may be represented by a set of Differential-Algebraic system of Equations (DAE) of the form:

$$\begin{aligned} \dot{x} &= f(x, y_1, y_2, u, \mu) \\ 0 &= g(x, y_1, y_2, u, \mu) \\ z &= h(x, y_1, y_2, u, \mu) \end{aligned} \tag{6}$$

Where x stands for generators dynamic state variables and their controls, defined by the nonlinear vector field f. The vector y_1 represents machines settings at generator buses, y_2 represents the set of algebraic variables, which typically correspond to load bus voltages and angles; μ stands for slow varying parameters, over which operators have no direct control, such as changing loading levels or photovoltaic power generation, and u represents the control settings that operators directly or indirectly control, such as reference voltages of AVRs, shunt compensation or PV power factor. The nonlinear algebraic function g describes the

algebraic equations that include power flow equations. The output variables are typically the reactive power generation at all generator buses, and active generation at the swing bus. They are described by a vector z defined by the nonlinear function h.

The static continuation power flow technique takes into account standard power flow models, i.e. constant PV or PQ generators with reactive power limits, and static PQ or voltage dependent loads. The interested reader can find a detailed description of the standard continuation power flow analysis in (Cãnizares, 2002). The stability information that can be obtained by the static continuation power flow is typically associated to the maximum loading margin of the system. However, since this paper focuses on photovoltaic penetration, the stability margin λ is defined in this paper as a measure of the maximum level of photovoltaic power generation.

$$\boldsymbol{P}_i^{PV} = \lambda \boldsymbol{P}_i^{max,\,PV} \tag{7}$$

This margin is limited by voltage stability limits (saddle-node bifurcation or limit-induced bifurcation) or security limits (voltage limits, transmission line thermal limits).

Saddle node bifurcation (SNB) is recognized as one of the most significant static factors for voltage stability problems in power system. According to Saddle-node bifurcation (Cãnizares, 1997):

$$\begin{aligned} & g(y,\lambda) = 0 \\ & \nabla_y g(y,\lambda) v = 0, \\ & \quad |v|=1 \end{aligned} \tag{8}$$

$$\begin{aligned} & g(y,\lambda) = 0 \\ & \nabla_y g(y,\lambda)^T w = 0 \\ & \quad |v|=1 \end{aligned} \tag{9}$$

where, w and v are the left and right eigenvectors respectively.

The effect of smooth parameter variations on the stability properties can be studied with continuation algorithms applied to the combined system of algebraic and differential equations (Equations 1-5) using a pseudo-arclength continuation strategy (Yakout, 1993). It also contains a number of routines which can be used to detect limit points and bifurcations as a function of a system parameter. The idea underlying a bifurcation analysis is to investigate qualitative changes in the system dynamics (e.g. stability loss, birth or death of oscillations, passage from periodic to chaotic solutions or vice versa, etc.) under slow variations of distinctive system parameters. This theory helps to predict how and when the system becomes instable. More detailed discussions about the stability of power systems DAE model are in (Guoyun *et al.*, 2005).

3.3. Load flow analysis

We simulate the impact of photovoltaic penetration on the voltage profile in the base case and the load flow results are given in Figures 6-8. The results show that the bus voltages for every node are within the acceptable range, *i.e.* between 0.93 p.u. and 1.07 p.u. and no overvoltage is detected as illustrated in Figure 6. The active powers injected at the different nodes are shown in Figure 7. The injected reactive powers are represented by the histogram in Figure 8. Note that all the reactive power consumption is supplied by the source 53 “Swing bus”.

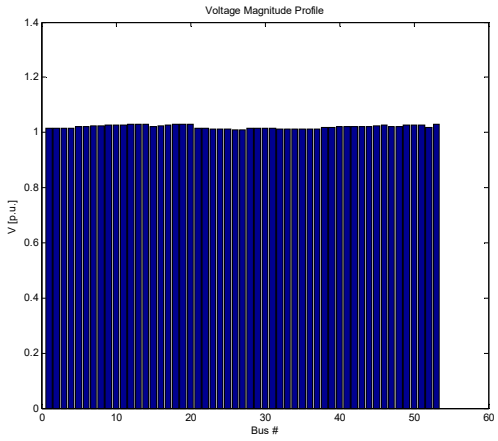

Figure 6. Voltage magnitude profile

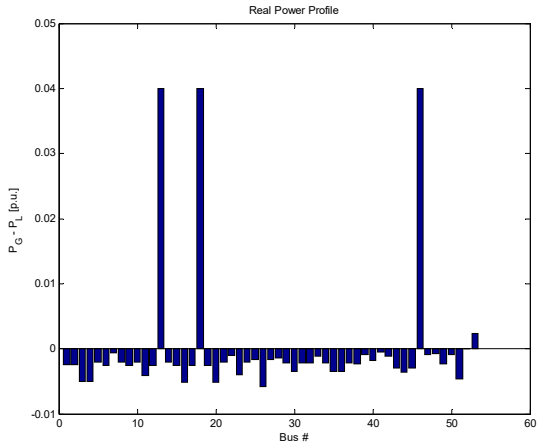

Figure 7. Real power profile

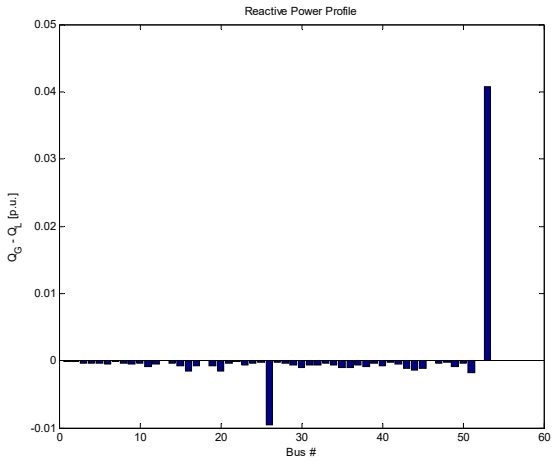

Figure 8. Reactive power profile

3.4. Impact of photovoltaic penetration on the voltage stability

3.4.1. Base Case

Figure 9 shows the bifurcation diagram at SPVG bus '13' and the most critical load bus "26" in the presence of the increasing photovoltaic generation margin λ. The voltage rises as the photovoltaic power injected increases to about λ ≈ 1.0 p.u. In this first half of the curve the voltage increases. This behavior is due to the fact that the feeder is decreasing its power injection into the distribution network.

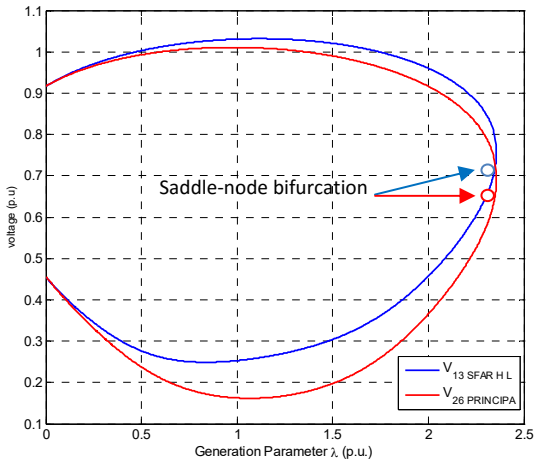

Figure 9. Bifurcation diagram of voltage at SPVG bus '13' and at load bus '26' as a function of the generation margin λ in base case

In the second half of the curve, the voltage decreases, as it is usual in nose curves. This happens because the feeder reverts its power flow and the photovoltaic farms are not only supplying local loads but also supplying power to the network. The system collapses at a saddle-node bifurcation for λ_{max} = 2.35 p.u, i.e 9.425 MW and therefore the maximum capacity of SPVGs that can be supported by the network is 28.2750 MW i.e 9.425 MW*3. Thus, the SNB is associated with maximum generation margin in the power flow models. The system becomes voltage instable at the operating point at which it's tangent to the system *PV* curve. This is equivalent to the singularity of the system Jacobian (Equation (6)).

3.4.2. System loading condition

To study the effect of system loading condition on the rate of the photovoltaic penetration, we considered a case corresponding to a load equal to half of the load of the network in the base case. Figure 10 shows the bifurcation diagram of voltage at photovoltaic bus "13" and the most critical load bus 26 function of the photovoltaic generation margin. The maximum penetration of the photovoltaic that can be supported by the network is 23.2MW i.e '7.73MW*3', (i.e 1.932 p.u*).

Comparing this result from the previous case when the network has a rated load (base case), there is a decrease in the margin from 28.2750 MW to 23.1900 MW, i.e a decrease of 18% compared to the base case. This is explained by the fact that in a lightly loaded network, the transit of powers is limited from the source to the loads and the penetration of photovoltaic sources implies a reversal of the direction of transit (SPVGs to the source station). This reversal will be faster if the network is low load which implies a lower penetration rates on holidays and Sundays. Thus, the maximum photovoltaic generation margin depends on the system loading condition.

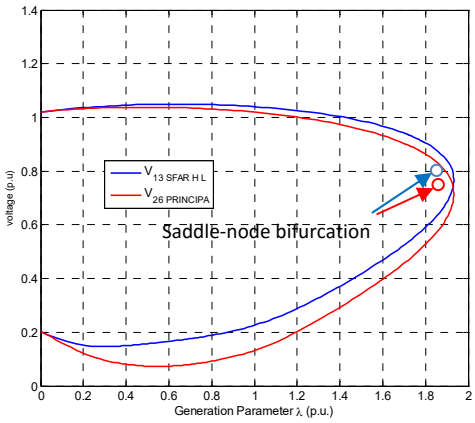

Figure 10. Bifurcation diagram of voltage at SPVG bus '13' and at load bus "26" as a function of the generation margin λ in lightly loaded case

For the base case, the slack bus provides active power to the grid as in this case the swing bus absorbs the power and seen its power is negative. The histogram in Figure 11 shows that from the point $\lambda \geq 0.5$, the swing bus reverse its injected power and become negative to the saddle node bifurcation point.

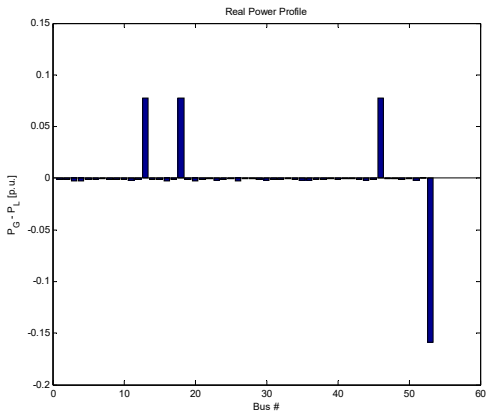

Figure 11. Real Power Profil at λ = 0.5 p.u

3.5. Dynamic performance

The focus here is to investigate the transient responses of the grid-connected photovoltaic generators and the synchronous network generators when a grid fault occurs. For this purpose, worst-case scenarios are considered in base case and in the maximum photovoltaic penetration. We first test the system transient response to a sudden group of photovoltaic power loss: disconnection of photovoltaic farm at bus "13". Then, disconnection of load is applied at a regular transmission network bus "26". Lastly, faulted voltage profiles are applied at the connection bus of the photovoltaic farm at bus '13' and the load bus '26'. The reactive power of the SPVGs is not plotted for all the simulation mentioned because the PV generator is operating at unity power factor and therefore the reactive power consumed or produced by the photovoltaic generator is equal to zero.

3.5.1. Base case

3.5.1.1 Perturbation 1: Disconnection of photovoltaic farm

The photovoltaic farm at bus '13' is abruptly disconnected from the network simultaneously by opening the circuit breakers. Immediately after the disconnection at t=20s, as a result of the photovoltaic generation loss, the synchronous rotor speed of swing bus dropped suddenly (Figure 12). The steady state rotor speed is about 47Hz corresponding to a significant frequency deviation of 3Hz which causes the loss by sub frequency of the machine. The disconnection causes a drop in the overall

network voltage profile. In particular, for the bus near to the photovoltaic islanded bus bus '12', the voltage undergoes a decrease of 2% of its rated voltage (Figure 13). By against, the variation of the voltage at photovoltaic bus "46", which remained connected to the network, is limited (less than 0.5% of nominal voltage).

The simulations results show that there is a strong relation between the terminal voltage of the PV generators and the rotor angle of the conventional generators. The scenario becomes worse as the photovoltaic penetration decrease. The disturbance in the bus terminal voltage directly affects the performance of the photovoltaic generator.

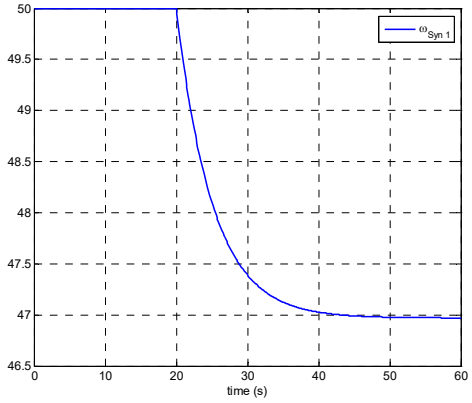

Figure 12. Variation of synchronous rotor speed at swing bus

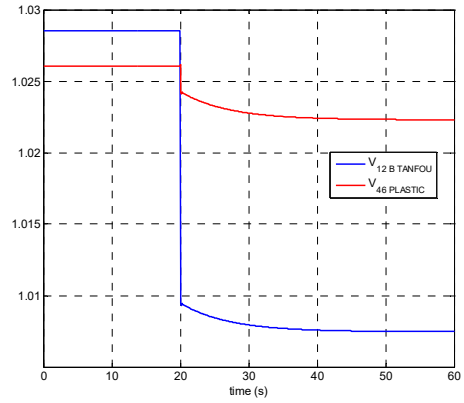

Figure 13. Variation of terminal voltage at PQ bus '12' and at SPVG bus'46'

3.5.1.2. Perturbation 2: Disconnection of load

The second disturbance scenario simulated corresponds to a loss of load at bus "26" (the most loaded bus), by opening the line at what this bus is connected. As the photovoltaic generators are of type SPQ and don't allow the voltage regulation, there has been a rise in voltage at the buses of the considered network. The voltage profile undergoes a 4% increase in the nominal voltage (Figure 14). The increase of the frequency due to this disturbance is of the order of 0.12 Hz which is acceptable and within the acceptable margin (Figure 15).

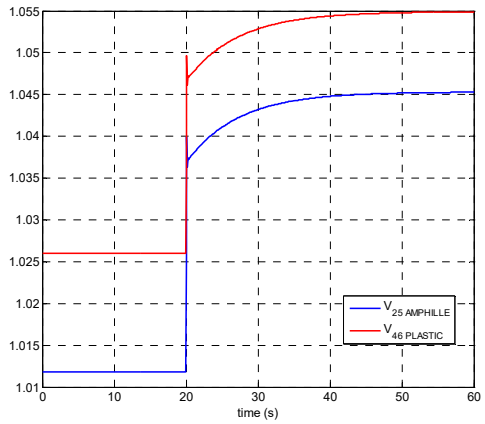

Figure 14. Variation of terminal voltage at SPVG 'bus 46' and load bus '25'

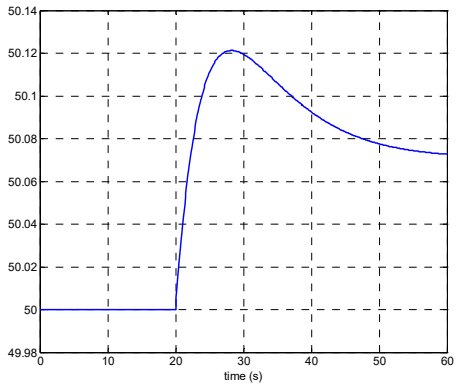

Figure 15. Variation of synchronous rotor speed at swing bus

3.5.1.3. Perturbation 3: Voltage dip faults at photovoltaic generator

The system performance to transient three-phase voltage dips is assessed. The reactive power requirements of photovoltaic farms are within a power factor unit. At t = 20s, a fault was applied at the connection bus of the photovoltaic generator at bus 13. The fault was cleared after 150 ms and the voltage has to drop 0.1 p.u.

Figure 16 shows the behavior of the photovoltaic generator during the fault-ride through. Immediately after the fault occurs, the voltage at the SPVG bus '13' drops to 0.1 p.u. Immediately after the fault is cleared at 20.15 s, the voltage at the SPVG terminal starts to rise and recovered to the steady state value of 1.0 p.u. The simulation results confirm that the SPVG controllers are capable of re-establishing the voltage at the photovoltaic terminal after the clearance of the short-circuit fault.

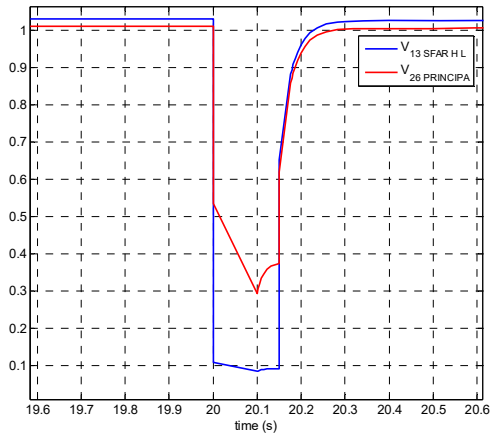

Figure 16. Variation of terminal voltage at SPVG bus "13" and load bus "26"

3.5.1.4. Perturbation 4: Network short-circuit

We have chosen the network bus "26', as the faulted bus, since it has exhibited weak static voltage. A three-phase short circuit is applied at t=20s, then cleared after 150ms. The resulting voltage profiles at photovoltaic generator of bus '13' and bus "26" are shown in Figure 17. We can see a significant voltage drop at the photovoltaic connection of bus 13 reaching 0.38p.u and at faulted bus, reaching down to 0.08p.u. The simulation results confirm that the SPVG controllers are capable of re-establishing the voltage at the photovoltaic terminal after the clearance of the short-circuit fault when a disturbance occur in the most loaded bus.

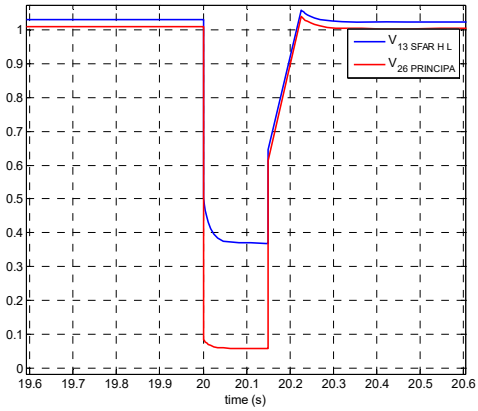

Figure 17. Variation of terminal voltage at SPVG bus "13" and load bus "26"

3.5.2. Case of maximum photovoltaic penetration

3.5.2.1. Perturbation 1: Disconnection of photovoltaic farm

The SPVG farm at bus '13' is abruptly disconnected from the network simultaneously by opening the circuit breakers. Immediately after the disconnection at t=20s, as a result of the PV generation loss, the synchronous rotor speed of swing bus dropped suddenly (Figure 18). The steady state rotor speed is about 41 Hz corresponding to a significant frequency deviation of 9 Hz which causes the loss by sub frequency of the machine.

The disconnection causes a drop in the overall network voltage profile. In particular, for the bus "12": the load bus near to the photovoltaic islanded bus; the voltage undergoes a decrease of 8% of its rated voltage (Figure 19). By against, the variation of the voltage at photovoltaic bus 46, which remained connected to the network, is 4% of its rated voltage.

The simulations results show that there is a strong relation between the terminal voltage of the photovoltaic generators and the rotor angle of the conventional generators. The scenario becomes worse as the photovoltaic generators are at maximum penetration. The disturbance in the bus terminal voltage directly affects the performance of the photovoltaic generator.

It can be concluded from Figures 18 and 19 that with higher photovoltaic penetration, disconnection of photovoltaic generators at bus '13' results in a significant frequency deviation in generator rotor angle and cause the system to be less transiently stable and could eventually lead to a bus voltage collapse.

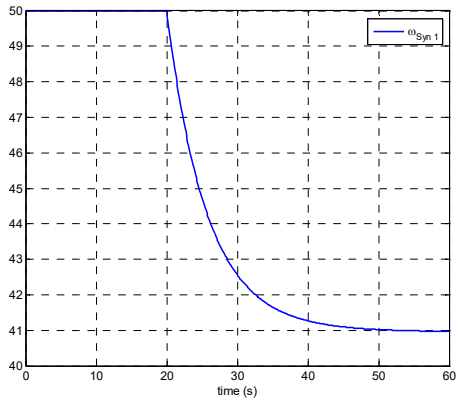

Figure 18. Variation of synchronous rotor speed at swing bus

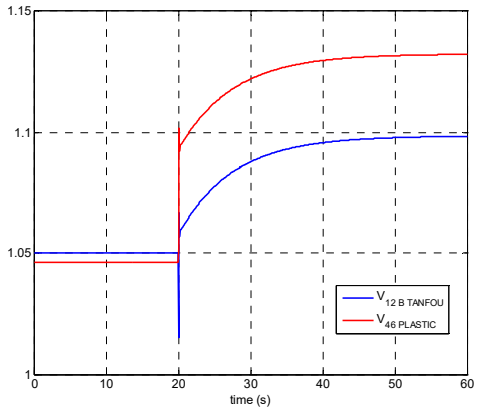

Figure 19. Variation of terminal voltage at SPVG bus "13" and load bus "26"

3.5.2.2. Perturbation 2: Disconnection of load

The second disturbance scenario simulated corresponds to a loss of load at bus "26" (the most loaded bus), by opening the line at what this bus is connected. As the photovoltaic generators are of type SPQ and don't allow the voltage regulation, there has been a rise in voltage at the buses of the considered network. The voltage profile undergoes a 4% increase in the nominal voltage Figure 20. The increase of the frequency due to this disturbance is of the order of 0.12Hz which is acceptable and within the acceptable margin (Figure 21).

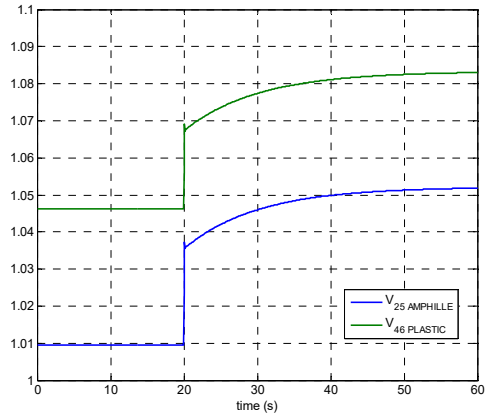

Figure 20. Variation of terminal voltage at SPVG bus "13" and load bus "26"

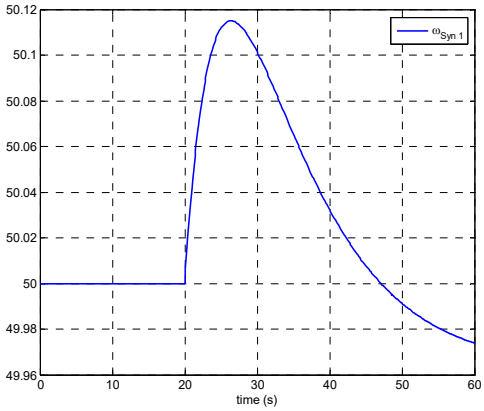

Figure 21. Variation of synchronous rotor speed at swing bus

3.5.2.3. Perturbation 3: Voltage dip faults at photovoltaic generator

The fault is applied at the connection bus of the photovoltaic and lasts 150 ms. Figure 22 shows the behaviour of the voltage at photovoltaic bus "13" and load bus "26" during the fault-ride through. Compared to the base case, the voltage dip occurs with a voltage off-peak level expressed in percent: $h_1 = 80\%$. Immediately after the fault occurs, the voltage at the photovoltaic bus and load bus drops significantly to 0.2 p.u and 0.5 p.u respectively. After the fault is cleared, the terminal voltage is recovered to the steady state value. The simulation results confirm that the SPVG controllers are capable of re-establishing the voltage at the photovoltaic terminal after the clearance of the short-circuit fault. The photovoltaic farms at bus "13", participate in supporting the network voltage.

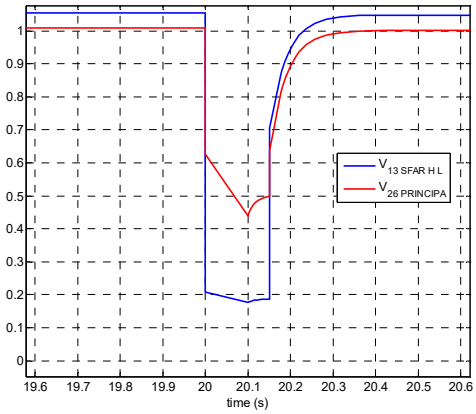

Figure 22. Variation of terminal voltage at SPVG bus '13' and load bus '26'

3.5.2.4. Perturbation 4: Network short-circuit

We have chosen the network bus "26", as the faulted bus, since it has exhibited weak static voltage. A three-phase short circuit is applied at t=20 s, then cleared in 150 ms. The resulting voltage profiles at buses 13 and 26 are shown in Figure 23. We can see a significant voltage drop at the SPVG connection of bus- reaching 0.50 p.u and at the faulted bus "26", reaching 0.1 p.u. Voltage regulation at SPVG bus is assured since the photovoltaic farms has been extended by a fast, continuously acting controller.

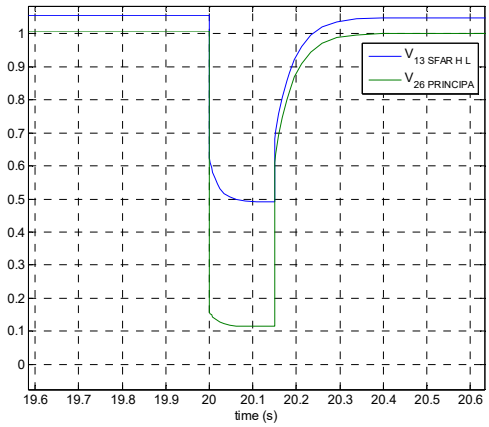

Figure 23. Variation of terminal voltage at SPVG bus '13' and load bus "26"

4. Conclusions

This paper investigated the dynamic performance of the radial Tunisian distribution networks integrating 12 MW photovoltaic energy. In this study, we noted a significant improvement in voltage profile due to the integration of photovoltaic farms. Voltage bifurcation diagrams indicated that with a high rate of photovoltaic energy, saddle-node bifurcation may occur. The maximum capacity of photovoltaic that can be supported by the Tunisian distribution network area in the southern suburbs of Tunis is 28.2750 MW in base case and 23.19 MW in case of holidays and Sundays i.e a decrease of 18% compared to the base case. This is explained by the fact that in a lightly loaded network, the transit of powers is limited from the source to the loads and the penetration of photovoltaic sources implies a reversal of the direction of transit of SPVGs to the source station. Thus, the maximum photovoltaic generation margin depends on the system loading condition.

The study of the static voltage stability of the network is completed by an analysis of transient stability. The total and instantaneous disconnection of the photovoltaic generators in the base and in the maximum solar penetration case is not without consequences on the stability of the power network that wants to maintain the greatest possible continuity of supply of photovoltaic energy on the network and participation in the setting of voltage and frequency. This disconnection resulted in a decrease in the frequency to values outside normal limits, resulting in the loss of frequency of all the connected machines.

Finally, the transient response of SPVGs to faults was discussed. The behavior of simulated solar farms into the Tunisian distribution network against the short-circuit failure shows the capacity of the photovoltaic farms variant to take better during voltage dips and can participate in the setting of the voltage. Therefore, these simulations demonstrate that these types of SPVGs are recommended to better meet the requirements of some network operators.

As a continuation to this work, we intend to extend this study to investigate the effects of different parameters of the photovoltaic generator: temperature and irradiance on the dynamic voltage stability of the grid using bifurcation diagrams.

References

Ajjarapu V. and Lee B. (1998). Bibliography on voltage stability. *IEEE Trans. on Power Syst*., vol. 13, p. 115-125.

Behnam T., Claudio C., and Kankar B. (2013). System Stability Impact of Large-scale and Distributed Solar Photovoltaic Generation: The Case of Ontario, Canada. *IEEE Transactions on Sustainable Energy*, vol.4, n°3, p. 680-688.

Canova A. Giaccone L. Spertino F. and Tartaglia M. (2009). Electrical impact of photovoltaic plant in distributed network. *IEEE Trans. Ind. Appl*., vol. 45, n° 1, p. 341-347.

CIGRE (2000). Modeling New Forms of Generation and Storage. *CIGRE, Tech. Rep*. TF 38.01.10.

Claudio C. (2002). Voltage Stability Assessment: Concepts, Practices and Tools. *IEEE/PES Power System Stability Subcommittee*, Final Document, Tech. Rep. SP101PSS, available at http://www.power.uwaterloo.ca.

Claudio C. (1997). Calculating Optimal System Parameters to maximize the distance to saddle-node bifurcations. *IEEE Transactions on circuits and systems-I: Fundamental theory and applications*. p. 1-27.

Erlich K.R. Shewarega F. (2006). Impact of large wind power generation on frequency stability. *In Proc. IEEE PES General Meeting*, Montreal, Quebec, Canada, p. 1-8.

Gautam D. Goel L. Ayyanar R. V. Vittal, Harbour T. (2011). Control strategy to mitigate the impact of reduced inertia due to doubly fed induction generators on large power systems," *IEEE Trans. Power Syst*., vol. 26, n° 1, p. 214-224.

Gautam D. Vittal V. Harbour T. (2009). Impact of increased penetration of DFIG-based wind turbine generators on transient and small signal stability of power system. *IEEE Trans. Power Syst*., vol. 24, n° 3, p. 1426-1434.

Guoyun C. Hill D.J. and Hui R. (2005). Continuation of local bifurcations for power system differential-algebraic equation stability model. *IEE Proc.-Gener. Transm. Distrib*., vol. 152, n° 4.

Haifeng L., Licheng J., David L., Chowdhury A. (2010). Impact of High Penetration of Solar Photovoltaic Generation on Power System Small Signal Stability. *International Conference on Power System Technology*.

IEEE Recommended Practice for Utility Interface of Photovoltaic (PV) Systems. (2000). *IEEE Std 929*.

Kakimoto N., Piao Q., Ito H., (2011). Voltage control of photovoltaic generator in combination with series reactor. *IEEE Trans. Sust. Energy*, vol. 2, n° 4, p. 374-382.

Ko H. S., Yoon G. G., Hong P. (2007). Active use of DFIG-based variable-speed wind-Turbine for voltage regulation at a remote location. *IEEE Trans. Power Syst*., vol. 22, n° 4, p. 1916-1925.

Lof P. A., Andersson G., and D. J. Hill. (1993). Voltage stability indices for stressed power systems. *IEEE Trans. on Power Sys*., vol. 8, p. 326-335.

Mohammed Masum Siraj K., Shamsul A., Ariful H., Nahid-Al-M. (2013). Stability analysis of power system with the penetration of photovoltaic based generation. *International Journal of Energy and Power Engineering*, vol. 2, n° 2, p. 84-89.

Marinopoulos A., Alexiadis M.C., Dokopoulos P. S. (2011). A correlation index to evaluate impact of PV installation on joule losses. *IEEE Trans. Power Syst*., vol. 26, n° 3, p. 1564-1572.

Milano F. (2005). Power System Analysis Toolbox. Documentation for PSAT version 2.1.9, available on www.power.unwaterloo.ca

Muljadi E., Butterfield C.P., Parsons B. and Ellis A. (2008). Effect of variable speed wind turbine generator on stability of a weak grid. *IEEE Trans. Energy Convers*., vol. 22, n° 1, p. 29-35.

NERC (2010). Standard Models for Variable Generation. *NERC special report*. draft. [Online]. Available: http://www.nerc.com

Paladin Design Base (2011). Photovoltaic Modeling. Power Analytics Corporation. 16870 West Bernardo Drive, Suite 330 San Diego, CA 92127 U.S.A.

Rakibuzzaman S., Nadarajah M., Ramesh B., Kwang Y. L., Abraham L. (2012). Influence of Large-scale PV on Voltage Stability of Sub-transmission System. *International Journal on Electrical Engineering and Informatics*, vol. 4, Number 1.

Ren (2014): Global Status Report. Renewable Energy Policy Network for the 21st Century. [Online]. Available: http://www.ren21.net

Thomson M., Infield D.G. (2007). Network power-flow analysis for a high penetration of distributed generation. *IEEE Trans. Power Syst*., vol. 22, n° 3, p. 1157-1162.

Wang Y. B., Wu C.-S., Liao H., Xu H.-H. (2008). Study on impacts of large-scale photovoltaic power station on power grid voltage profile. *Third International Conference on Electric Utility Deregulation, Restructuring and Power Technologies*.

WECC Wind Generation Development. (2010). *NREL, Tech. Rep*.

Xu X., Huang Y., He G., Zhao H., Wang W., (2009). Modeling of large-scale grid integrated PV station and analysis its impact on grid voltage. *International Conference on Sustainable Power Generation and supply*.

Yakout M. (1993). Suggested Techniques for Voltage Stability Analysis. Printed in the U.S.A. by the *IEEE Power Engineering Society*.

Yun Tiam T. (2007). Impact on the Power System of a Large Penetration of Photovoltaic Generation. *Power Engineering Society, IEEE General Meeting - PES*, p. 1-8.

Yun Tiam T., Kirschen D. S., and Jenkins N. (2004). A model of PV generation suitable for stability analysis. *IEEE Trans. Energy Conversion*, vol. 19, n° 4, p. 748-755.

Received: 8 June 2015
Accepted: 4 March 2016